Variational Blind Deconvolution of Multi-Channel Images

Ran Kaftory Yehushua Y. Zeevi

Department of Electrical Engineering
Technion
Haifa 43000, Israel

Nir Sochen

Department of Mathematics
tel-Aviv University
Tel-Aviv 69978, Israel

Abstract

The fundamental problem of de-noising and de-blurring images is addressed in this study. The great difficulty in this task is due to the ill-posedness of the problem. We suggest to analyze multi-channel images to gain robustness and to regularize it by the Polyakov action which provides an anisotropic smoothing term that use intra-channel information. Blind de-convolution is then solved by additional anisotropic smoothing term of the same type. It is shown that the Beltrami regularizer leads to better results than the Total Variation (TV) regularizer. An analytic comparison to the TV method is carried out and results on synthetic and real data are demonstrated.

1. Introduction and Previous Work

Noisy images are a practical reality that pose a challenge to any front-end of an imaging or vision system. Noise is introduced due to thermal fluctuations in sensors, quantization effects and properties of communications channels. Blurring occurs due to scattering of the light (e.g. atmosphere turbulence), optical limitations and motion. The widely-used model of spatially-invariant linear blurring operator and additive Gaussian noise is adopted in this study, to account for the blurring phenomena and the noise characteristics .

Denoting by $u^a(x,y) \quad a = 1,\ldots,d$ the source color channels of an image, the observed degraded color channel $z^a(x,y)$ is modelled as:

$$z^a = h * u^a + n \ , \tag{1}$$

where $h(x,y)$ is a blurring kernel acting on u^a by convolution, n is a Gaussian white noise and $a = r,g,b$ in the RGB color space.

One method, used for reconstructing a gray value image, is the Total Variation (TV) blind de-convolution [3]. This method suggests simultaneous recovery of the sharp denoised image and its blurring kernel. The recovery process is based on minimization of the functional:

$$\begin{array}{l} \min\limits_{u,h} f(u,h) \equiv \\ \min\limits_{u,h}\{\frac{1}{2}\left\|h*u-z\right\|^2 + \alpha_1 TV(u) + \alpha_2 TV(h)\} \ , \end{array} \tag{2}$$

where the norm in the data term is in the sense of the L^2 norm. The TV regularization operator is defined as:

$$TV(u) = \int |\nabla u| dxdy \ , \tag{3}$$

and it was successfully used for edge preserving image denoising [9].

A more general regularization operator was recently introduced in the context of a general Beltrami framework for low level vision [10] . According to this framework, color images are represented as surfaces in R^5, with the coordinates (x,y,u^r,u^g,u^b). A metric is introduced for measuring distances on the surfaces, and minimization of the Polyakov action, adopted from high energy physics, yields the Beltrami operator. In an Euclidean space, the Polyakov action (along with the induced metric) measures the surface area. Minimizing it causes the image to become smoother, its color channels to co-orient and align and, consequently, its edges to be preserved and match in position, unlike the the results of reconstruction by considering the three color channels independently.

In this paper the approach of minimizing a functional, resembling that of eq. (2), is combined with the Polyakov action as a regularization operator, in order to deblur and denoise a blurred color image contaminated by Gaussian noise. The functional to be minimized is:

$$\begin{array}{l} \min\limits_{u^a,h} f \equiv \\ \min\limits_{u^a,h}\{\frac{1}{2}\sum\limits_a \left\|h*u^a-z^a\right\|^2 + \alpha_1 S(u^a) + \alpha_2 S(h)\}, \end{array} \tag{4}$$

where the norms are in the L^2 sense and S is the Polyakov action. Minimizing eq. (4) with respect to u^r, u^g, u^b and

h, recovers the image color channels and the blurring kernel, simultaneously. The parameters α_1 and α_2 control the smoothness of the solution.

Alternatively we will alternate the minimization of the image and the Blurring kernel such that the following free energies are minimized:

$$\min_{\mathbf{u}} f_u(\mathbf{u}; h, \mathbf{z}) \equiv \min_{u^a}\{\tfrac{1}{2}\sum_a \|h * u^a - z^a\|^2 + \alpha_1 S(\mathbf{u})\}, \quad (5)$$

$$\min_{h} f_h(h; \mathbf{u}, \mathbf{z}) \equiv \min_{h}\{\tfrac{1}{2}\sum_a \|h * u^a - z^a\|^2 + \alpha_2 S(h)\}, \quad (6)$$

The paper is organized as follows: we first introduce the main ideas regarding the Beltrami framework i.e. the representation of color images as two-dimensional surfaces embedded in a five-dimensional space, the induced metric for measuring distances on the surface and the Polyakov action, which measures the surface area. The numerical scheme for minimizing eq. (4) (or equivalently eqs. (5, 6)), which is similar to the alternating minimization scheme, described in [3], is then presented. The Beltrami operator is incorporated into the Euler-Lagrange equations, by modifying the regularization parameters (or by adding a functional [7]). The equations are linearized by the fixed-point lagged diffusive method, discussed in [18], and solved using the conjugate gradient method. The regularization parameters are then selected to provide the best possible results.

Finally, the properties of the Beltrami-based restoration are analyzed and illustrated by examples, and its advantages over other techniques are discussed.

2 Images as surfaces embedded in a higher dimensional space

A color image is represented according to the Beltrami framework [8] as a two-dimensional surface embedded in a 5-dimensional 'spatial-feature' space via the "Monge patch" $\left(X^1, X^2, X^3, X^4, X^5\right) = \left(x, y, u^r, u^g, u^b\right)$. The blurring kernel can be similarly represented as a two-dimensional surface embedded in a three-dimensional 'spatial-feature' space (x, y, h). The distance, ds, on the image surface, measured as a function of the local coordinates on the surface, is defined as follows:

$$ds^2 = g_{11}dx^2 + 2g_{12}dxdy + g_{22}dy^2 \ , \quad (7)$$

where $G = (g_{\mu\nu})$ is a metric, calculated using the pullback procedure described in [11] which is defined as follows:

Let $X : \Sigma \rightarrow M$ be an embedding of Σ in M, where M is a Riemannian manifold with a metric $(g_{ij})_M$. We can use the knowledge of the metric on M and the map X to construct the metric on Σ. This procedure is called the pullback procedure and is given as follows:

$$(g_{\mu v})_\Sigma(\sigma^1, \sigma^2) = (g_{ij})_M(X(\sigma^1, \sigma^2))\partial_\mu X^i \partial_v X^j \ , \quad (8)$$

where i,j = 1,...,dimM are being summed over, and $\partial_\mu X^i \equiv \frac{\partial X^i(\sigma^1,\sigma^2)}{\partial \sigma^\mu}$.

For the two-dimensional surface it is given explicitly as:

$$\begin{aligned} g_{11} &= \sum_{a=1}^{n}\sum_{b=1}^{n} k_{ab}\frac{\partial X^a}{\partial x}\frac{\partial X^b}{\partial x} \\ g_{12} = g_{21} &= \sum_{a=1}^{n}\sum_{b=1}^{n} k_{ab}\frac{\partial X^a}{\partial x}\frac{\partial X^b}{\partial y} \\ g_{22} &= \sum_{a=1}^{n}\sum_{b=1}^{n} k_{ab}\frac{\partial X^a}{\partial y}\frac{\partial X^b}{\partial y} \ , \end{aligned} \quad (9)$$

where n is the dimension of the embedding space, and k_{ab} is its metric. Defining k_{ab} for the embedding color space, and for the embedding blurring kernel space, as (see other interesting options in [13]):

$$k_{ab} = \begin{cases} \delta_{ab} & a, b = 1, 2 \\ \beta^2\delta_{ab} & elsewere \ , \end{cases} \quad (10)$$

and using the pullback procedure, the metric $G = g_{\mu\nu}$ can be calculated for the color surface and the blurring kernel surface respectively:

$$G_{rgb} = \begin{pmatrix} 1 + \beta^2\sum_a (u_x^a)^2 & \beta^2\sum_a u_x^a u_y^a \\ \beta^2\sum_a u_x^a u_y^a & 1 + \beta^2\sum_a (u_y^a)^2 \end{pmatrix}$$
$$G_h = \begin{pmatrix} 1 + \beta^2 u_x^2 & \beta^2 u_x u_y \\ \beta^2 u_x u_y & 1 + \beta^2 u_y^2 \end{pmatrix} \quad (11)$$

The Polyakov action is defined for a generally defined metric embedding X^a and metric G as

$$S(X^a) = \int dxdy\sqrt{\det G}\sum_{ab}\nabla X^a G^{-1}\nabla X^b k_{ab} \quad (12)$$

The modified Gradient Descent equations for this functional are [12]:

$$X_t^a = \Delta_G X^a = \frac{1}{\sqrt{\det(G)}}\nabla\left(\sqrt{\det(G)}G^{-1}\nabla X^a\right) \ , \quad (13)$$

where $X_t^a \equiv \frac{\partial X^a}{\partial t}$.

For gray-valued and color images and their induced metrics, as described above, the functional eq. (12) is reduced to an area functional:

$$S(u^a) = \int \sqrt{\det G_{rgb}}dxdy =$$
$$\int \sqrt{1 + \beta^2\sum_a(|\nabla u^a|^2) + \tfrac{1}{2}\beta^4\sum_{ab}(\nabla u^a, \nabla u^b)^2}dxdy \quad (14)$$

$$S(h) = \int \sqrt{\det G_{ker}} dxdy = \int \sqrt{1 + \beta^2 \left|\nabla h\right|^2} dxdy \ , \tag{15}$$

where $(\nabla u^a, \nabla u^b)$ stands for the magnitude of the vector product of ∇u^a and ∇u^b.

3 Beltrami based restoration

The Polyakov action is used as a regularization operator for both the color image and its blurring kernel. The functional to be minimized is as follows:

$$\begin{array}{l} \min\limits_{u^a,h} f \equiv \min\limits_{u^a,h}\{\frac{1}{2}\sum\limits_a \left(\left\|h * u^a - z^a\right\|^2\right) + \\ \alpha_1 \int \sqrt{\det(G_{rgb})} dxdy + \alpha_2 \int \sqrt{\det(G_{\ker})} dxdy\} \ , \end{array} \tag{16}$$

The Euler-Lagrange equations for eq. (16), with respect to u^a and h, are:

$$\begin{array}{l} \frac{\delta f}{\delta h} = \sum\limits_a (u^a(-x,-y) * (h * u^a - z^a)) - \\ \qquad \alpha_2 \nabla \cdot (\sqrt{\det(G_{\ker})} G_{\ker}^{-1} \nabla h) = 0 \\ \frac{\delta f}{\delta u^a} = h(-x,-y) * (h * u^a - z^a) - \\ \qquad \alpha_1 \nabla \cdot (\sqrt{\det(G_{rgb})} G_{rgb}^{-1} \nabla u^a) = 0 \ , \end{array} \tag{17}$$

with the boundary conditions: $\frac{\partial u^a}{\partial n} = 0$ and $h(x,y) = 0$ for $(x,y) \in \partial\Omega$, where $\partial\Omega$ is the boundary of the kernel domain and n is the normal to the image on the boundaries of the image domain.

Since the extent of regularization is controlled by the regularization parameter, we want to diminish it near the edges. Since the term $\sqrt{\det(G)}$ is basically an edge indicator, we can use a similar idea to the adaptive TV minimization presented in [14] and replace the regularization parameters α_1 and α_2 with the terms:

$$\begin{array}{l} \alpha_1(x,y) \rightarrow \frac{\alpha_1}{\sqrt{\det(G_{rgb})}} \\ \alpha_2(x,y) \rightarrow \frac{\alpha_2}{\sqrt{\det(G_h)}} \ . \end{array} \tag{18}$$

The new definitions of the regularization parameters α_1 and α_2 introduce the natural generalization of the Laplacian from flat spaces to manifolds, the so-called second order differential parameter of Beltrami to be denoted by Δ_G:

$$\begin{array}{l} \frac{\delta f}{\delta h} = \sum\limits_a u^a(-x,-y) * (h * u^a - z^a) - \alpha_2 \Delta_{\ker}(h) = 0 \\ \frac{\delta f}{\delta u^a} = h(-x,-y) * (h * u^a - z^i) - \alpha_1 \Delta_{G_{rgb}}(u^a) = 0 \ , \end{array} \tag{19}$$

with the boundary conditions as in (17) where $\Delta_G(X) = \frac{1}{\sqrt{\det(G)}} \nabla \cdot \sqrt{\det(G)} G^{-1} \nabla X$.

The functional $f(u^r, u^g, u^b, h)$ in eq. (16) is not jointly convex. But, for a given u^r, u^g and u^b it is convex with respect to h. For a given u^g, u^b and h, $f(\cdot, u^b, u^g, h)$ is a convex function with respect to u^r and similarly for u^g and u^b. This enables the adaptation of the alternating minimization scheme, which was found to be robust and fast [2].

These equations (19) can be derived alternatively by minimizing two functionals. Similarly, the image and the kernel are described as surfaces embedded in a higher dimensional Euclidean space. The metric of the Euclidean space is k_{ab} as described above. The fidelity term is defined then *on the manifold*:

$$\begin{array}{l} \min\limits_{u^a,h} f_u \equiv \min\limits_{u^a}\{\frac{1}{2}\sum\limits_a \int dxdy \sqrt{G_{rgb}} \left\|h * u^a - z^a\right\|^2 + \\ \qquad \alpha_1 \int dxdy \sqrt{\det(G_{rgb})} G_{rgb}^{ij} \nabla_i X^a \nabla_j X^a\} \ , \end{array} \tag{20}$$

$$\begin{array}{l} \min\limits_{u^a,h} f_h \equiv \min\limits_{h}\{\frac{1}{2}\sum\limits_a \int dxdy \sqrt{G_{\ker}} \left\|h * u^a - z^a\right\|^2 + \\ \qquad + \alpha_2 \int dxdy \sqrt{\det(G_{\ker})} G_{\ker}^{ij} \nabla_i X^a \nabla_j X^a\} \ , \end{array} \tag{21}$$

The modified Euler-Lagrange equations are:

$$\begin{array}{rcl} \frac{1}{\sqrt{G_{rgb}}} \frac{\delta f_u}{\delta u^a} & = & 0 \\ \frac{1}{\sqrt{G_{\ker}}} \frac{\delta f_h}{\delta h} & = & 0 \end{array} \tag{22}$$

and are identical to eq. (19). Note that the fidelity term is weighted in these functionals by a locally dependent factor. This means that at each point the relation between the smoothing part and the fidelity part is different. In particular the fidelity to the measurements is enforced strongly at points with high gradients where the determinant of the metric is large. Larger deviations from the observations is permissable at points with low gradients. In the modified Euler-Lagrange equations the factor $\sqrt{\det G}$ is shifted to the smoothing term. This amounts for an adaptive smoothing mechanism: At points of large gradients the smoothing term is suppressed and fidelity of the restored image to the observed values is enforced. Larger smoothing is allowed to take place at points of low gradient values.

The minimization scheme is stated as follows: Take as initial guess, $u^{a_0} = z^a$ and $h^0 = \delta(x,y)$. Assume we have u^{a_n} and h^n, and solve for h^{n+1}:

$$\begin{array}{l} \sum\limits_a u^{a_n}(-x,-y) * (h^{n+1} * u^{a_n} - z^a) - \\ \qquad \alpha_2 \Delta_{\ker}(h^{n+1}) = 0, \end{array} \tag{23}$$

and impose the following conditions over the solution: $\int\limits_\Omega h^{n+1}(x,y)dxdy = 1$, $h^{n+1}(x,y) = h^{n+1}(-x,-y)$, $h^{n+1}(x,y) \geq 0$, and $h^{n+1}(x,y) = 0$ for $(x,y) \in \partial\Omega$.
Solve for $u^{a_{n+1}}$:

$$h^{n+1}(-x,-y) * (h^{n+1} * u^{a_{n+1}} - z^a) - \alpha_1 \Delta_{G_{rgb}}(u^{a_{n+1}}) = 0g \tag{24}$$

and impose the following condition over the solution: $u^{a_{n+1}}(x,y) \geq 0$

The proposed algorithm can be modified to solve first for $u^{a_{n+1}}$ and then for h^{n+1}. The Euler-Lagrange equations are linearized using the fixed point lagged diffusive method, introduced in [18] and solved using the conjugate gradient methods described in [4].

4 The regularization parameters

The parameter β, introduced in the induced metric in section 2, interpolates between the Euclidean L_1 and Euclidean L_2 norms. Since the Euclidean L_2 norm penalizes discontinuities, and therefore prefers smooth restoration, we explore the more interesting case of a large β (Euclidean L_1 norm).

The regularization parameters α_1 and α_2 control the balance between goodness of fit of $h * u^a$ to the measured data z^a and the amount of regularization with respect to the Polyakov action of u^a and h. Intuitive, analytic, and numerical considerations can lead to the choice of values for the regularization parameters for the restored color image and the blurring kernel.

4.1 The parameter α_1

As was described earlier, the Polyakov action measures the surface area of the manifold. Color image is a two-dimensional surface embedded in a five-dimensional space. Minimizing its surface area will de-noise the image, since noise is a feature with very large surface area in comparison to its scale.

The first step of the restoration scheme can be solving eq. (24) first and then eq. (23). Inserting the initial guess $h^0 = \delta(x,y)$, eq. (24) yields:

$$(u^{a_1} - z^a) - \alpha_1 \Delta_{G_{rgb}}(u^{a_1}) = 0 \ . \qquad (25)$$

The problem in this step is reduced to finding the best regularization parameter for de-noising a color channel u^{a_1} when blur is not introduced.

In [6] this parameter was found to be proportional to the noise variance and by numerical experiments, it was found that setting it to the noise variance is adequate.

4.2 The parameter α_2

Unlike the case of the regularization parameter α_1, where the problem was reduced to finding the best regularization parameter for denoising a color image when blur is not introduced, the case for finding the regularization parameter α_2 is not that simple. The analytic tools used so far for finding the regularization parameter for the color image are not adequate for finding the best regularization parameter for the kernel. Intuition and previous work [3] suggest that the parameter does not depend on the noise level of the image, but depends on the extent of the desired deblurring.

Experiments show that there is a wide range of values for α_2 (from 0.01 to 0.05) that estimates the same kernel. Within this range, the estimated kernel depends only on the extent of blurring affecting the observed image [6]

5 Results

The proposed algorithm was found to be robust. It converges after only 5 iterations. Figures 1-4 illustrates examples of restoring Gaussianly blurred, moving and 'out of focus' blurred and noisy images, using the regularization parameters determined in the previous section. Observe how the restored images are sharp and noiseless, and the estimated blurring kernels resemble the true kernels.

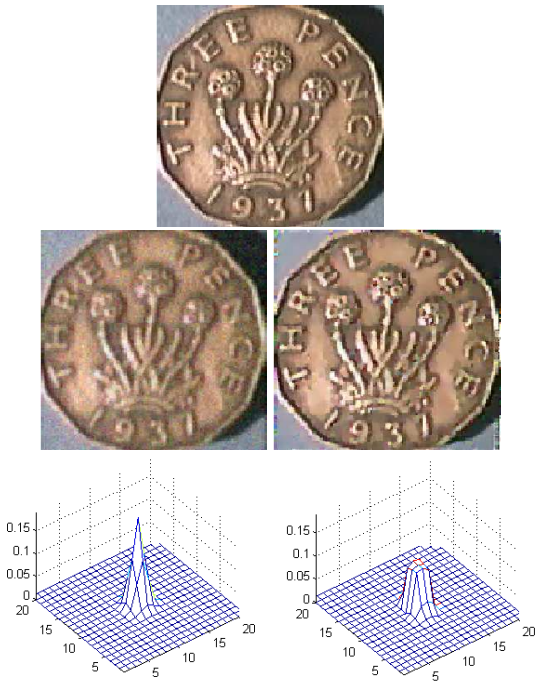

Fig. 1 Radially symmetric blur. From left to right - 1st row: Original. 2nd row: Blurred and noisy image, restored image. 3rd row: true and estimated kernels.

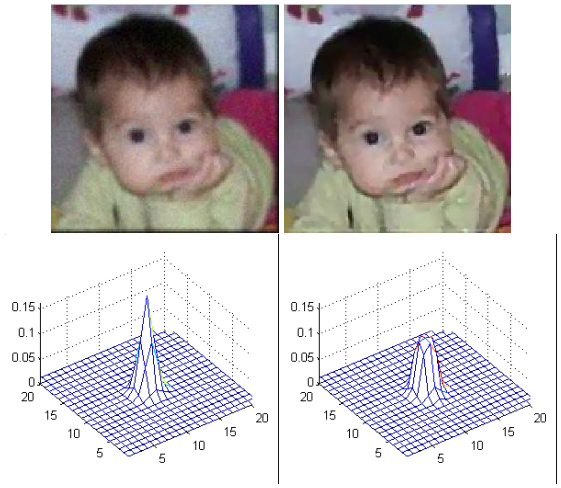

Fig. 2 Radially symmetric blur. From left to right - 1st row: Original. 2nd row: Blurred and noisy image, restored image. 3rd row: true and estimated kernels.

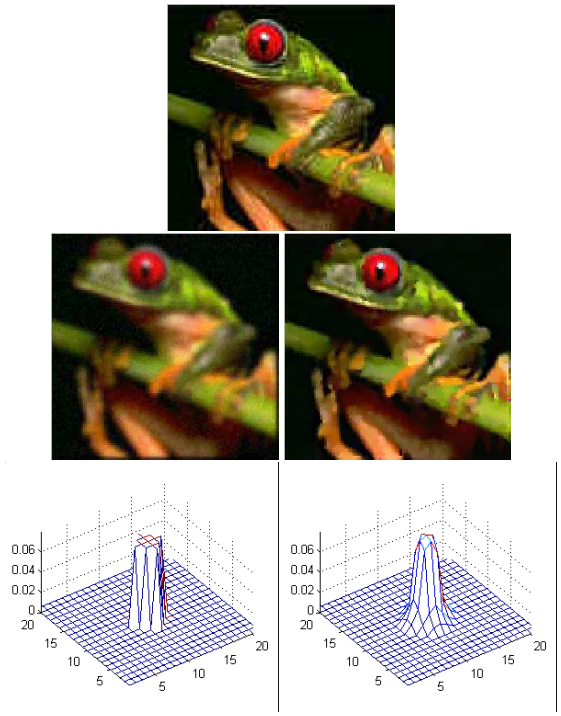

Fig. 3 Out of focus blur. From left to right - 1st row: Original. 2nd row: Blurred and noisy image, restored image. 3rd row: true and estimated kernels

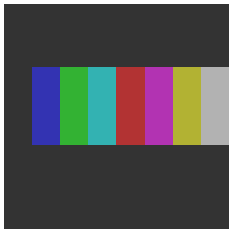

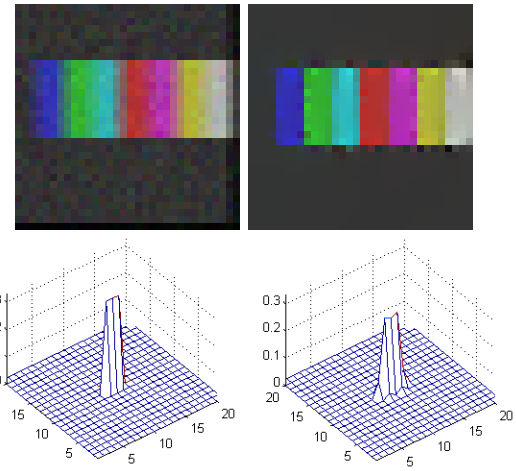

Fig. 4 Motion blur. From left to right - 1st row: Original. 2nd row: Blurred and noisy image, restored image. 3rd row: true and estimated kernels

A quantitative measure of the error, associated with the estimation of the color image and of the blurring kernel, can be obtained by calculating the peak signal-to-noise ratio (PSNR):

$$\text{PSNR(X)} = 20 \log \sqrt{\frac{3 \cdot N \cdot M}{\sum_a \sum_{j=1}^{N} \sum_{k=1}^{M} (X^a_{j,k} - \hat{X}^a_{j,k})^2}}$$

where X stands for u^a or h, and N · M is the number of pixels. Table 1 summarizes the PSNR of the images in figures 1-4.

Image	**Observed Image PSNR**	**Restored Image PSNR**	**Restored Kernel PSNR**
Coin	21 dB	23 dB	60 dB
Baby	28 dB	32 dB	62 dB
Frog	25 dB	27 dB	59 dB
Color Bar	24 dB	31 dB	47 dB

Table 1: PSNR of the restored images and kernels

6 Properties of the Beltrami-based restoration

The properties of restoration of a two-dimensional surface, embedded in a three-dimensional 'spatial-feature' space, similar to the case of gray value images (or the blurring kernel), is explored first. The Polyakov action in equation (14), becomes for a large β the modified Total Variation operator defined in [18]:

$$\begin{aligned} S(h) = \int \sqrt{1 + \beta^2 (\nabla h)^2} dx dy = \\ \beta \int \sqrt{\gamma^2 + (\nabla h)^2} dx dy = \beta TV(h) \ . \end{aligned} \tag{26}$$

where $\gamma = \frac{1}{\beta}$.

Since the Total Variation does not penalize discontinuities or smooth functions, it was used successfully as a regularization operator in reconstructing gray-valued images [9], [3]. Reconstruction using the Total Variation operator was explored in [15] and

yielded the following properties: Edges are preserved in the reconstructed image; The intensity change of image features is proportional to the regularization parameter, and inversely proportional to the feature scale; Small-scale details, like noise, are smoothed out, leaving a sharp noiseless reconstruction. In the Beltrami-based restoration, the regularization parameter α_1 is replaced in the Euler-Lagrange equation by $\frac{\alpha_1}{\sqrt{\det(G)}}$, yielding an adaptive Total Variation restoration [16]. Since the term $\frac{\alpha_1}{\sqrt{\det(G)}}$ is basically an edge indicator, it assumes small values in the presence of an edge, while in smooth areas, where the gradients are very close to zero, its values increase up to one. This feature overcomes the problems of the intensity reduction near edges, and of elimination of small scale features. To illustrate this property, consider the simple R^1 function:

$$u(x) = \begin{cases} 0.2 & x \in \Omega_1 \\ 0.8 & x \in \Omega_2 \\ 0.2 & x \in \Omega_3 \end{cases} , \tag{27}$$

.

A Gaussian noise is added to this function to produce the noisy function:

$$z(x) = u(x) + n \tag{28}$$

.

Experiment with the Beltrami based restoration algorithm on this noisy function suggests that the restored function should be

$$u(x) = \begin{cases} 0.2 + \delta_1 & x \in \Omega_1 \\ 0.8 + \delta_2 & x \in \Omega_2 \\ 0.2 + \delta_3 & x \in \Omega_3 \end{cases} , \tag{29}$$

where δ_i is the intensity change in region i. The restoration problem is:

$$\begin{aligned} &\min_u \{\tfrac{1}{2}\|u - z\|^2 + \alpha_1 \beta TV(u)\} = \\ &\min_{\delta^i} \{\sum_i (|\Omega_i|\,\delta_i^2) + \alpha_1\beta(0.6 + \delta_2 - \delta_1 + 0.6 + \delta_2 - \delta_3)\} \end{aligned} , \tag{30}$$

where $|\Omega_i|$ is the length of region i. Minimizing eq. (30) by derivation with respect to δ^i yields:

$$\begin{aligned} \delta_1 &= \tfrac{\alpha_1\beta}{|\Omega_1|} \\ \delta_2 &= -\tfrac{2\alpha_1\beta}{|\Omega_2|} \\ \delta_3 &= \tfrac{\alpha_1\beta}{|\Omega_3|} \end{aligned} . \tag{31}$$

Therefore, in the restored function $u(x)$, the intensity change is directly proportional to the parameter α_1 and inversely proportional to the scale. This result was presented in [16] for the Total Variation based restoration.

For simplicity, let assume that $|\Omega_1| = |\Omega_3|$ and therefore $\delta_1 = \delta_3$. Modifying the regularization parameter α_1 to $\frac{\alpha_1}{\sqrt{\det(G)}} = \frac{\alpha_1}{\sqrt{1+\beta^2|\nabla u|^2}}$, introduces the Beltrami operator to the solution. The regularization parameter can be explicitly expressed by:

$$\frac{\alpha_1}{\sqrt{1+\beta^2\left|\nabla u\right|^2}} = \begin{cases} \frac{\alpha_1}{\sqrt{1+\beta^2(0.6+\delta_2-\delta_1)^2}} & x \in \partial 12 \\ \frac{\alpha_1}{\sqrt{1+\beta^2(0.6+\delta_2-\delta_1)^2}} & x \in \partial 23 \\ \alpha_1 & elsewhere \end{cases} , \tag{32}$$

where $\partial 12$ stands for the boundary of region 1 and 2, and $\partial 23$ stands for the boundary of region 2 and 3.

Considering only the boundary points and implementing the modified α_1, eq. (31) becomes:

$$\begin{aligned} \delta_1 &= \tfrac{\alpha_1\beta}{|\Omega_1|\sqrt{1+\beta^2(0.6+\delta_2-\delta_1)^2}} \quad (\,on\ \partial 12) \\ \delta_2 &= -\tfrac{2\alpha_1\beta}{|\Omega_2|\sqrt{1+\beta^2(0.6+\delta_2-\delta_1)^2}} \quad (\,on\ \partial 12) \\ \delta_2 &= -\tfrac{2\alpha_1\beta}{|\Omega_2|\sqrt{1+\beta^2(0.6+\delta_2-\delta_1)^2}} \quad (\,on\ \partial 23) \\ \delta_3 &= \tfrac{\alpha_1\beta}{|\Omega_1|\sqrt{1+\beta^2(0.6+\delta_2-\delta_1)^2}} \quad (\,on\ \partial 23) \end{aligned} . \tag{33}$$

Since β is assumed to be very large, equation (33) can be approximated:

$$\begin{aligned} \delta_1 &= \tfrac{\alpha_1}{|\Omega_1|(0.6+\delta_2-\delta_1)} \quad (\,on\ \partial 12) \\ \delta_2 &= -\tfrac{2\alpha_1}{|\Omega_2|(0.6+\delta_2-\delta_1)} \quad (\,on\ \partial 12) \\ \delta_2 &= -\tfrac{2\alpha_1}{|\Omega_2|(0.6+\delta_2-\delta_1)} \quad (\,on\ \partial 23) \\ \delta_3 &= \tfrac{\alpha_1}{|\Omega_1|(0.6+\delta_2-\delta_1)} \quad (\,on\ \partial 23) \end{aligned} . \tag{34}$$

Since $\delta_1 = \delta_3$ the solution to (34) is:

$$\begin{aligned} \delta_1 &= \tfrac{0.6|\Omega_1||\Omega_2| - \sqrt{|\Omega_1|^2|\Omega_2|^2 0.36 - 4|\Omega_2|(|\Omega_1||\Omega_2| + 2|\Omega_1|^2)\alpha_1}}{2(|\Omega_1||\Omega_2| + 2|\Omega_1|^2)} \\ \delta_2 &= -\tfrac{0.6|\Omega_1||\Omega_2| - \sqrt{|\Omega_1|^2|\Omega_2|^2 0.36 - 4|\Omega_2|(|\Omega_1||\Omega_2| + 2|\Omega_1|^2)\alpha_1}}{(|\Omega_2|^2 + 2|\Omega_1||\Omega_2|)} \end{aligned} . \tag{35}$$

In this case, intensity change δ_i is not directly proportional to the regularization parameter α_1 or inversely proportional to the scale in the boundary points. In fact the intensity change is minimal.

The function z is actually divided into 2 types of regions. Step regions in which the intensity change is defined in (35), and smooth regions in which the parameter $\frac{\alpha_1}{\sqrt{1+\beta^2|\nabla u|^2}} \approx \alpha_1$ and the intensity change are defined in equation (31).

Restoration of the function u using the Total Variation operator and the Beltrami operator are shown in Fig. 5. Gaussian noise with variance 0.05 was added to the function u. The size of the regions is $|\Omega_1| = |\Omega_3| = 25$, $|\Omega_2| = 10$, $\alpha_1 = \frac{1}{60}$ and $\beta = 60$.

The Total Variation restoration should yield:

$$\begin{aligned} \delta_1 = \delta_3 &= \tfrac{\alpha_1\beta}{25} = 0.04 \\ \delta_2 &= -\tfrac{\alpha_1\beta}{5} = -0.2 \end{aligned} , \tag{36}$$

and the Beltrami-based restoration should yield:

$$\begin{aligned} \delta_1 = \delta_3 &= \tfrac{150 - \sqrt{22500 - 60000\alpha_1}}{3000} = 0.001 \\ \delta_2 &= -\tfrac{150 - \sqrt{22500 - 60000\alpha_1}}{600} = -0.005 \end{aligned} . \tag{37}$$

Observe the contrast reduction between Ω_1 and $\Omega_2/3$ in the Total Variation based restoration (caused by the direct relation to

the smoothing parameter α_1). The value of Ω_2 is extensively reduced due to its small scale (caused by the inverse relation to the feature scale). In the Beltrami-based restoration the change in the contrast is hardly seen due to the wick relation to α_1 and the feature scale. The numerical results as seen in Fig 5 match perfectly with the analytic prediction of eq. (36) and (37).

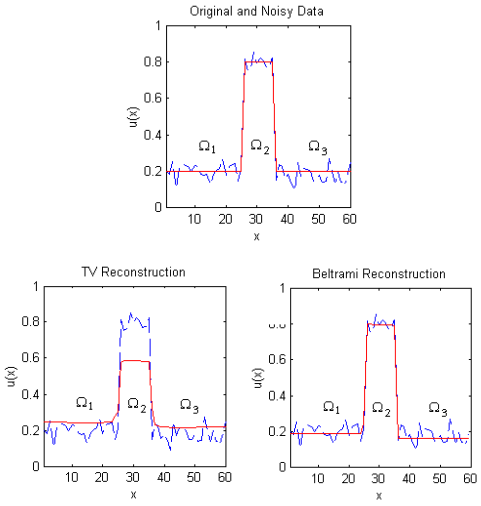

Fig. 5 Up: original noisy image. Down-left: After denoising by total variation. Down-right: After denoising with the Beltrami operator

As mentioned in section 2, the Polyakov action for a two-dimensional surface embedded in a five-dimensional 'space-feature' space as in the case of a color image is:

$$S(u^i) = \int \sqrt{G_{rgb}} dxdy =$$

$$\int \sqrt{1 + \beta^2 \sum_a (|\nabla u^a|^2) + \tfrac{1}{2}\beta^4 \sum_{ab} (\nabla u^a, \nabla u^b)^2} dxdy \ , \tag{38}$$

where $(\nabla u^a, \nabla u^b)$ stands for the magnitude of the vector product of the vectors ∇u^a and ∇u^b. While minimizing the Polyakov action, the term $1 + \beta^2 \sum_a |\nabla u^a|^2$ regularizes each color channel as described in the gray value case earlier. The term $\beta^4 \sum_{ab} (\nabla u^a, \nabla u^b)^2$, which is more dominant in the limit of a large β, measures the directional difference of the gradients between color channels. The minimization of the Polyakov action takes care, therefore, of the alignment and location matching of the edges over the three channels. To illustrate this, a noisy color image was produced by a digital camera (Fig. 6 up-left). The angles between the orientations of the gradient in the noisy image are plotted by arrows (Fig. 6 down-left). When an arrow points right the angle is zero (the gradients are of the same orientation). A Beltrami-based restoration is illustrated on the up-right side of Fig. 6. Note that in the original image the gradient of the channels do not align together, the image looks noisy and the edges are not sharp. In the restored image, however, the angles between the gradient orientations are reduced (Fig. 6 down-right) and the restored image looks sharper and less noisy.

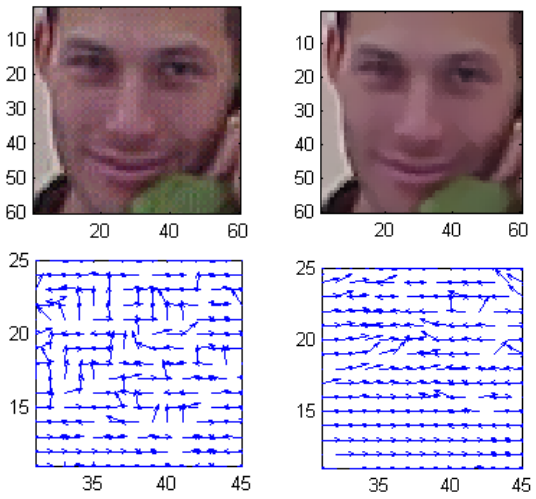

Fig. 6 Up - down, left to right: Original noisy image, de-noised image, the angles between colors gradients before, and after the de-noising process.

Color image reconstruction is hardly addressed, due to the common belief that color image reconstruction can be treated as reconstructing three gray valued independent channels. This is a wrong assumption in applications where the human visual system (HVS) is the receiver. The HVS is very sensitive to the slightest edge miss-alignment, or to intensity reduction in one of the color channels. In [1], the color TV was defined as a regularization operator for the restoration of vector valued images. A coupling between the color channels was achieved through the regularization parameter, assigning small regularization parameter to channels with smaller Total Variation. In the reconstructed color image, "weaker" channels are smoothed less and therefore preserve the intensity relationship between the channels. In the Beltrami-based restoration a coupling between the color channels is introduced not only through the regularization parameter, but also through the regularization operator itself. Comparison between the best color TV reconstruction and the best Beltrami-based reconstruction of a noisy image, where blur is not introduced, is depicted in Fig. 7. Table 2 summarized the PSNR of these images. Observe how in both of the reconstructed images, the noise is removed completely. However, only in the Beltrami-based reconstruction the edges are sharp and visually satisfying and color artifacts are not introduced. The blur and color artifacts in the TV process is caused probably because of misalignment of the edges in the different color channels (see [17] for a full explanation of this phenomenon).

7 Concluding remarks

Using the Beltrami operator in the objective functional, and adopting the alternating minimization scheme for minimizing eq. (4), yields a robust algorithm for simultaneous recovery of a blurred noisy color image and of its blurring kernel. The parameters α_1 and α_2 of this process are automatically selected to yield the good results. The restored images depict sharp edges and gradients of the channels well align. The RGB color space was adopted in this study. However, the approach can be just as well incorporate the

HVS color coordinates [19]. The HVS color space was shown to be effective in spatio-chromatic image enhancement. Another issue to be further explored relates to question of what is the 'right' metric for measuring distances in the higher dimensional space. Further such insight will most likely improve the results of the proposed approach to image deblurring and denoising.

Fig. 7 Left to right, top to bottom: Original, noisy, TV and Beltrami images.

Observed Image PSNR	**TV Restored PSNR**	**Beltrami restored PSNR**
23 dB	29 dB	30 dB

Table 2: PSNR of the TV and Beltrami restored image

8 Acknowledgement

Research supported in part by the Ollendorff Center, the Adams Brain Super-Center, The Israeli Academy of Science and the ONR-MURI Research

References

[1] P. Blomgren and T. Chan, "Color TV: Total Variation Method for Restoration of Vector Valued Images", IEEE Transactions on Image Processing, Vol. 7, pp. 304-309, 1998.

[2] T. Chan and C. Wong, "Convergence of the Alternating Minimization Algorithm for Blind Deconvolution", UCLA Math Department, CAM Report 99-19, June, 1999.

[3] T. F. Chan and C. Wong, "Total Variation Blind Deconvolution", IEEE Transactions on Image Processing, Vol. 7, pp. 370-375, March 1998.

[4] M. Hankle, "Conjugate Gradient Type Methods for Ill-Posed Problems", Universitat Karlsruhe, Longman Scientific & Technical, England, pp. 13, 1995.

[5] J. Immerkaer, "Fast Noise Variance Estimation", Computer Vision and Image Understanding, Vol. 64, No. 2, pp. 300-302, 1996.

[6] R. Kaftory, "Color Image Reconstruction Using the Beltrami Framework", MSc Thesis, Technion-Israel Institude of Technology, 2001.

[7] R. Kaftory, N. Sochen and Y. Y. Zeevi, Technical report in preparation.

[8] R. Kimmel, R. Malladi and N. Sochen, "Images as Embedded Maps and Minimal Surfaces: Movies, Color, Texture and Volumetric Medical Images", International Journal of Computer Vision, Vol. 39 (2), pp. 111-129, 2000.

[9] L. Rudin, S. Osher and E. Fatemi, "Nonlinear Total Variation Based Noise Removal Algorithms", Physica D., 60, pp. 259-268, 1992.

[10] N. Sochen, R. Kimmel and R. Malladi, "A General Framework for Low Level Vision", IEEE Transactions on Image Processing, Vol. 7, no. 3, pp. 310-318, March 1998.

[11] N. Sochen, R. Kimmel and R. Malladi, "From High Energy Physics to Low Level Vision, Lecture Notes in Computer Science: First International Conference on Scale-Space Theory in Computer Vision", Springer-Verlag, 1997.

[12] N. Sochen, R. Kimmel and R. Malladi, "A General Framework for Low Level Vision", *IEEE Trans. in Image Processing, Special Issue on Geometry Driven Diffusion*, 7 (1998) pp. 310–318.

[13] N.Sochen, and Y. Y. Zeevi, "Representation of colored images by manifolds embedded in higher dimensional non Euclidean space", Proceedings of ICIP98, pp. 166-170, Chicago, 1998.

[14] D. Strong, P. Blomgren and T. Chan, "Spatially Adaptive Local Feature-Driven Total Variation Minimizing Image Restoration", UCLA Math Department, CAM Report 97-32, July, 1997.

[15] D. Strong and T. Chan, "Edge-Preserving and Scale-Dependent Properties of Total Variation Regularization", UCLA Math Department, CAM Report 00-38, October, 2000.

[16] D. Strong. "Adaptive Total Variation Minimizing Image Restoration, Ph.D. Dissertation", UCLA Math Department, CAM Report 97-38, August, 1997.

[17] D. Tschumperlé, PhD Thesis. University of Nice Dec. 2002.

[18] C. Vogel and M. Oman, "Iterative Methods for Total Variation Denoising", SIAM Journal of Scientific Computing, Vol. 17, pp. 227-238, 1996.

[19] S. G. Wolf, R. Ginosar and Y. Y. Zeevi, "Spatio-Chromatic Image Enhancement Based on a Model of Human Visual Information Processing", J. Visual Communcation and imge Representation, Vol. 9, pp. 25-37, 1996.